JOURNAL OF RAMAN SPECTROSCOPY, VOL. 26, 535–551 (1995)

Solvent and Frequency Dependence of Vibrational Dephasing on Femtosecond Time-Scales

P. Vöhringer,* R. A. Westervelt,† T.-S. Yang, D. C. Arnett, M. J. Feldstein and N. F. Scherer‡
Department of Chemistry, University of Pennsylvania, Philadelphia, Pennsylvania 19104-6323, USA

The results of degenerate wavenumber third-order polarization (pump–probe) measurements of vibrational dephasing and relaxation in a variety of solvents are reported. The 20 fs duration pulses are sufficiently short to allow the preparation and detection of vibrational coherences (i.e. wavepackets) to 800 cm^{-1} oscillator wavenumber. The high quality of the pump–probe data permits the unique determination of eight underdamped modes for the cyanine dye under study. The relaxation of the underdamped modes does not show a significant solvent dependence. The relaxation mechanisms that give rise to loss of vibrational coherence and to the solvent-dependent relaxation of low-wavenumber (<100 cm^{-1}) modes are discussed. The wavenumber dependence of the vibrational dephasing rate varies with a scaled exponential dependence $\exp(-\omega/\omega_0)$, or equally well with the inverse square of the vibrational wavenumber. The exponential form would imply that vibrational dephasing occurs by population relaxation. The latter form, however, may imply higher order coupling between the bath and solute through the solute vibrational anharmonicity such that the off-diagonal contributions to the prepared wavepacket relax by pure dephasing. Exponentially decaying contributions to the pump–probe signal are found to arise from overdamped modes that are excited by the short laser pulses as opposed to a solvation response. The solvent-dependent relaxation of these overdamped modes is determined to be similar to diffusive unimolecular barrier crossing dynamics observed in dense media.

INTRODUCTION

A central question in the study of chemical reaction dynamics in solution is understanding the role of the solvent in affecting, facilitating or even initiating the chemical event. The unique qualities of reactions occurring in liquids are the intermolecular interactions that affect the way a chromophore moves and exchanges energy and momentum with the surrounding solvent. The solvent bath serves as an energy source or a dissipative force at different times during the reactive process. These properties are conventionally known as solvent friction.[1] For example, the finite inertia of a (polar) solvent will produce a wavenumber-dependent frictional drag during barrier crossing in electron-transfer reactions.[2] Therefore, the appropriate way to view chromophore–solvent interactions is in terms of the time-scales on which the friction (collisional and dielectric) influences the chromophore.

Nonlinear spectroscopy has proved to be a powerful technique for studying molecular properties in condensed media.[3] Ideas for the femtosecond domain were based on the earlier work that described impulsive effects in resonant studies on the picosecond time-scale.[4] The rapid development of short-duration laser pulses has allowed the study of molecular dynamics directly on the time-scale of vibrational motion or elementary chemical step.[5–9] An interesting aspect of femtosecond pulse non-linear spectroscopy is that measurements transcend simply quantifying rates of processes with greater precision to recovering spectroscopic information via the preparation and detection of non-stationary superposition states (i.e. vibrational wavepackets). The ability of broadband excitation to prepare and detect the evolution of coherent vibrational superposition states has been demonstrated for large (i.e. dye) molecules in solution.[10–12] Nelson and Ippen[13] exploited femtosecond non-resonant 'impulsive' spectroscopy to examine the dynamics of neat liquids in a transient grating geometry. McMorrow *et al.*[14] examined the linearized third-order polarization response in impulsive birefringence. These experiments and their theoretical description showed that the evolution of the impulsively prepared vibrational wavepacket may result in sinusoidal modulation of the amplitude of the detected signal. The recorded amplitude (or phase) modulation of the probe beam as a function of pump–probe time delay reflects the Bohr wavenumbers of the medium.

Recently, time-domain measurements of the vibrational spectrum of both the optically coupled ground and excited electronic states of small reactive molecular solutes has become possible.[7–9,15] The oscillatory motion of vibrational wavepackets reflects the persistence of coherence in the chromophore. Fourier transformation of such waveforms gives the vibrational level spacings of the Franck–Condon optically active mode(s). In the case of resonant experiments, this gives spectral information even in the absence of structure in the linear absorption spectrum. This is an important capability since the linear absorption spectra of even

* Deutsche Forschungsgemeinshaft Postdoctoral Fellow.
† Department of Education GAANN Predoctoral Fellow.
‡ National Science Foundation National Young Investigator.

CCC 0377-0486/95/070535-17

small molecules in solution are broadened or even structureless, thus precluding traditional analysis.

Two-, three- and four-pulse experiments can be treated as four-wave mixing processes, where the pump and probe pulses combine in the sample to create a non-linear polarization that, in turn, radiates an electric field.[3,16] A non-linear response function description of the third-order polarization, $P^{(3)}$, shows[3] that the time evolution operators for a solute–solvent system probed by different types of spectroscopy contain complementary information about the time correlation function of solvent fluctuations (i.e. librations, vibrations, translations). The microscopic dynamics of the solvent are reflected in the relaxation of solute vibrational and electronic phase and energy. The evolution of electronic[17,18] and vibrational[19] phase reflects the form of the chromophore–bath interaction potentials and the correlation time of solvent fluctuations. The coherence of the chromophore at some time after excitation is determined by the correlation function of the solvent (librational) frequency modulation and the magnitude of the coupling of the chromophore excitation coordinate to the bath.[3] Microscopic friction originates in the coupling of solvent motions to the chromophore dynamics along the solvation, dephasing or reaction coordinates. Therefore, the evolution of chemical reactions is expected to depend on the wavenumber response of the solvent.

Elucidation of the solvent time correlation functions that are relevant to chemical reactions in solution requires combining information from different types of non-linear spectroscopic measurements. In this paper we focus on vibrational dephasing and relaxation as made manifest through impulsive pump–probe spectroscopy. In another paper, we investigate optical dephasing of the same chromophore and solvents studied by two-pulse photon echo techniques.[20] The pump–probe data are essential for analysis of the chromophore vibrational motions that contribute to optical dephasing and will be discussed here. Independently performed pump–probe studies[21] of the same chromophore in ethylene glycol exhibit only the lowest frequency oscillation reported here.

We performed pump–probe measurement on a cyanine dye chromophore in a variety of solvents with sufficiently short duration pulses to prepare vibrational coherences to 800 cm^{-1} wavenumber. In the Experimental section we describe the laser system and experimental apparatus used in these studies. The sample is the cyanine dye molecule 1,1′,3,3,3′,3′-hexamethylindotricarbocyanine iodide (HITCI) dissolved in protic and aprotic solvents. As will be seen in the Results section, these very short pulse (20 fs duration) experiments are able to extract temporal and spectral information. The prompt exponential relaxation of the pump–probe signal shows a pronounced solvent dependence consistent with relaxation of overdamped low-frequency modes. We also measured vibrational dephasing of eight modes of the dye molecule in a variety of solvents. The number of well defined oscillators is sufficient to obtain a functional form for the wavenumber dependence of the dephasing rate. In the Discussion section IV we consider the multiplicity of dynamic processes that contribute to the third-order polarization response.

EXPERIMENTAL

The femtosecond pulse laser system used in these studies consists of an argon ion laser (Coherent 310) pumped Ti-doped sapphire oscillator. The laboratory-built Ti:sapphire laser (4.5 mm rod, fused-silica prisms with 60 cm spacing) is based in part on the design of Krausz *et al.*[22] and routinely produces 20 fs duration pulses as judged from both interferometric and intensity autocorrelations. The pulses are coupled out of the non-dispersive end of the X-fold cavity[23] and, after prism (pre-)compensation, are found to be Fourier transform limited and without wings and satellites in time or spikes in the spectrum. Shorter duration but somewhat chirped pulses could be produced.

A schematic diagram of the laser and experimental arrangement is shown in Fig. 1. A fused-silica prism arrangement is used to precompensate for the group velocity dispersion resulting from dielectric coatings, beam splitters and lenses and to optimize the pump–probe autocorrelation at the sample. The probe beam is an s-polarized first surface reflection from a fused-silica substrate and is variably delayed with respect to the pump. The beams are directed parallel to the sample and focused with a $f = 6$ cm achromat lens. The sample,

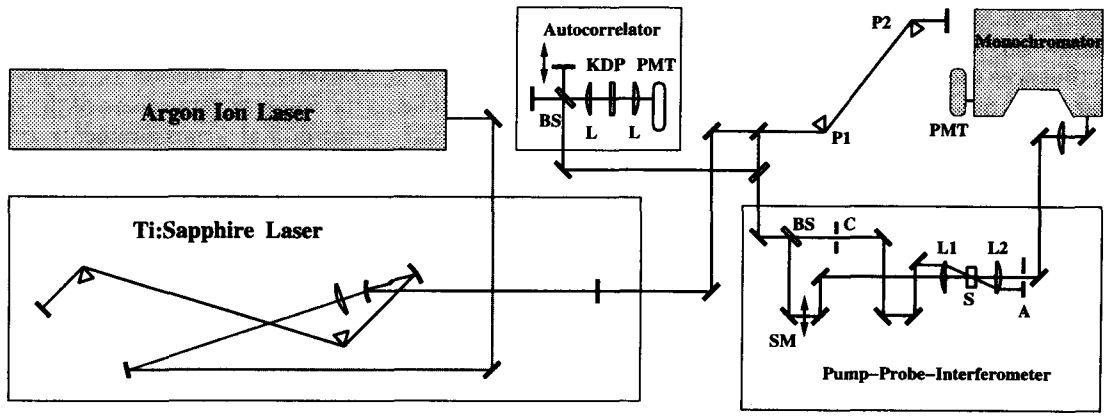

Figure 1. Schematic diagram of the experimental apparatus. BS = beam splitter; PMT = photomultiplier tube; P1, P2 = pulse compression prisms; SM = scanning delay line; C = chopper; S = sample jet; L1, L2 = 6 cm focal length achromat lenses; A = aperture.

5×10^{-5} M HITCI (Kodak) in ethylene glycol (Fisher, HPLC grade), is flowed as a 100–150 μm thick jet to minimize thermal heating and lensing effects and has an optical density of less than 0.3 at 770 nm. All measurements are performed at 295 K.

The energies of the pump and probe pulses at the sample are 1–2 nJ and 50–100 pJ, respectively. In all measurements reported here the pump and probe beams have parallel relative polarization. A mechanical chopper is used to amplitude modulate the pump beam. The probe beam is directed on to a photodiode or photomultiplier (PMT) and the pump-induced modulation of the pulse intensity is phase-sensitively detected and processed in a digital lock-in amplifier (Stanford SR-850) referenced to the chopper modulation. The lock-in signal is recorded for each 4 fs step of the optical delay line (0.25 s accumulation per point) and approximately ten scans of 1000 points are averaged together. The pump–probe dynamics of HITCI in other solvents including alcohols, water and acetonitrile were also examined.

The method of linear prediction singular value decomposition[24] analysis (LPSVD) was used to determine the parameters for the exponentially damped cosinusoidal terms that describe the data set. This method of analysis has been used to determine the wavenumbers, phases and time constants of vibrational wave packets of dye molecules[24] and molecular iodine in solution.[8] Standard non-linear least-squares approaches to data fitting are not very reliable owing to the number of parameters involved. As described below, a biexponential decay plus offset is fitted to the data and the fitted curve is subtracted prior to analysis of the oscillatory signals. Thus the LPSVD analysis need only consider oscillatory contributions to the signal. The experimental scans were recorded and analyzed on a 486 IBM-compatible computer.

RESULTS

Figure 2 shows the linear absorption and emission spectra of HITCI in ethylene glycol solution. The spectrum of the Ti:sapphire laser pulses is superimposed on the molecular spectra showing overlap with the low-energy portion of the absorption spectrum and most of the steady-state emission spectrum. The emission spectrum is obtained from a dilute solution in a fluorescence cuvette with excitation at the absorption maximum. Inspection of the data gives a steady-state Stokes-shift of 440 cm^{-1}. It is shown below that both absorptive and emissive transitions between the ground and first excited singlet state contribute to the pump–probe signals.

Several groups have examined the long-time kinetics of HITCI via flash photolysis, transient absorption and thermal grating spectroscopy.[25–28] According to these studies, a transient absorption from S_1 to S_n occurs near 780 nm while isomerization yields a photoisomer with an absorption near 850 nm. The excited state level kinetics coupling the different states, $S_1 \rightarrow S_0$, $S_1 \rightarrow PI$ and $S_1 \rightarrow T$, where PI and T are the photoisomer and triplet manifold of states, have also been established. With the exception of an $S_1 \rightarrow S_n$ absorption, all of these processes are slow on the few picosecond time-scale; the S_1 excited state lifetime is 1.2 ns and the quantum yield for PI formation is 12%. This means that isomerization also does not contribute measureably to relaxation on the few picosecond time-scale. The data shown below are consistent with a bleach and/or stimulated emission response; transient absorption is not a significant contribution to the signals shown here. A dominant transient absorption from S_1 would result in a pump–probe signal of opposite sign (i.e. negative) to

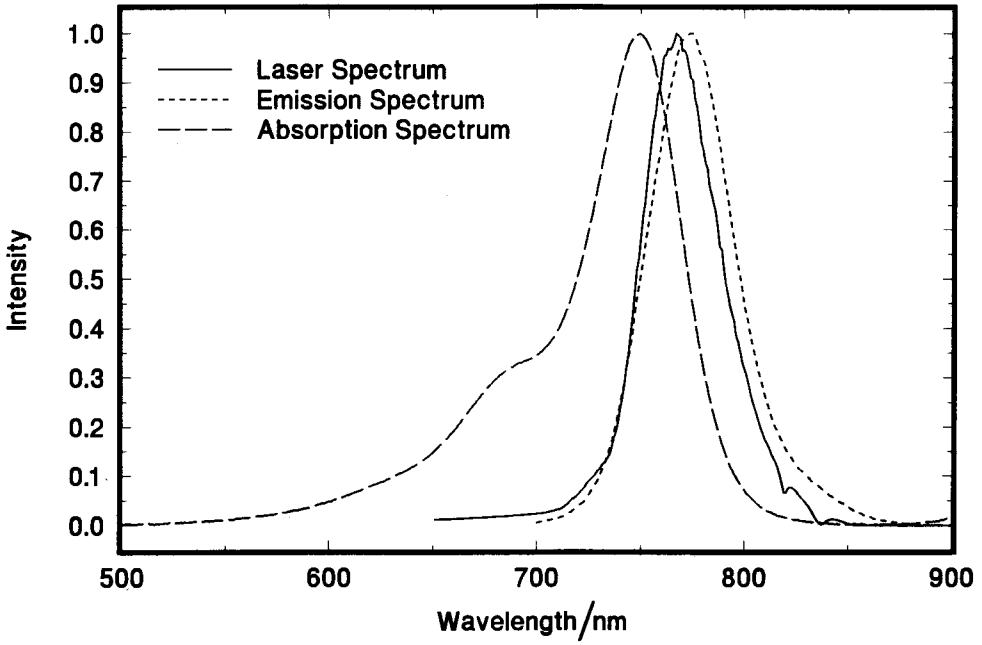

Figure 2. Absorption (long dashed line) and emission (short dashed line) spectra of HITCI in ethylene glycol. The spectrum of the laser pulse (solid line), which spans both absorption and emission bands, is superimposed.

that observed.* Therefore, the possible dynamic processes that contribute to the pump–probe signals shown below are (i) coherence decay of impulsively prepared ground and excited state vibrational wavepackets, (ii) vibrational population relaxation within the S_0 and S_1 singlet electronic states and (iii) solvation resulting from changes in the solute dipole moment on optical excitation.

Pump–probe signals

The optically induced (pump) modulation of the probe transmission of HITCI in ethylene glycol excited and probed by 35 fs Gaussian pulses centered at 780 nm is shown in Fig. 3(a). A positive signal indicates increased probe intensity. Also shown in this figure is the intensity autocorrelation of these pulses (i.e. cross-correlation of pump and probe). The pump-induced modulation of the probe transmission rises with the integral of the autocorrelation. Oscillations of the transmitted intensity are evident after the pump–probe overlap (<40 fs delay) and coherent artifact contribution.[21,29,30] The prominent oscillation occurs with a period of 220 fs which corresponds to a vibrational level spacing of *ca.* 150 cm^{-1}. The inset to the figure gives an expanded view of the oscillatory and rapidly decaying portion of the pump–probe signal. The long-lived component of the signal (i.e. offset) corresponds to the depletion of the ground-state population and to the population of S_1 following electronic excitation by the pump pulse. The optically induced (pump) modulation of the probe transmission of HITCI in ethylene glycol excited and probed by 22 fs Gaussian pulses centered at 780 nm is shown in Fig. 3(b). The pump–probe signal is recorded over a 4 ps delay time. The most obvious difference between this third-order polarization response from that shown in Fig. 3(a) is the increased richness of oscillatory contributions to the signal, some of which persist for several picoseconds.

The procedure for data analysis begins by fitting the data sets with a biexponential decay and offset prior to analysis of the oscillatory components. Figure 3(c) shows an expanded view of the pump–probe signal of HITCI in decanol. The two curves passing through the data are single and biexponential best fits. The biexponential decay functions gives a better approximation to the waveform than a single exponential decay as deduced from the residual of the fit; this is true for all of the solvents investigated. Because of the finite time resolution of the experimental apparatus and possible coherent coupling artifact contributions to the signal, the data fitting is started at 40 fs delay for all solvents. The fast decay parameter is the same for the ethylene glycol data sets of Fig. 3(a) and (b) with a value of $\tau_1 = 200 \pm 50$ fs. The offset accounts for the 100 ps to nanosecond time-scale 'decay' resulting from rotational reorientation, electronic relaxation and isomerization dynamics.[25–29] The fast component is the only one that is well determined over the 2–4 ps time range of the scans.

The time constants from single and biexponential fitting of the HITCI pump–probe signal in all solvents studied are summarized in Table 1. Longer time scans are required to establish more accurately the time constant of the slower component. Inspection of the τ_1 and τ_2 data in Table 1 shows that both time constants scale reasonably well with solvent viscosity. Some deviations from this trend are observed but probably reflect the fact that the long time constants are comparable to the length of the measurement and are therefore not very precisely determined.

Fourier spectrum and vibrational coherence

The fitted biexponential decay function is subtracted from the original data and the resultant oscillatory waveform is Fourier transformed and normalized to the laser autocorrelation response to obtain the (absolute magnitude) spectrum. These spectra, shown in Fig. 4(a) and (b), correspond to the time domain data of Fig. 3(a) and (b), respectively. In both cases well defined peaks occur at 120, 160, 300, 400, 500 and 550 cm^{-1}. Smaller amplitude features also appear at 40, 90, 220, 650 and 800 cm^{-1}, especially in Fig. 4(b). The more prominent high-wavenumber features in Fig. 4(b) reflect the larger spectral bandwidth of the shorter duration pulses. The Fourier components at 400 cm^{-1} and above have all been identified in cw Raman spectra as ground-state vibrational modes.[31] The measurements reported here are, of course, preparing and detecting coherent superposition states of various vibrational modes. The resulting Fourier transformed spectra reflect the energy differences (i.e. Bohr wavenumbers) characterizing the vibrational level spacing for different modes. In all cases the time-domain data presented in the figures and used

Table 1. Exponential fitting parameters for HITCI in various solvents[a]

Solvent	τ/ps	τ_1/ps	τ_2/ps	Viscosity/cP[b]
Acetonitrile	0.29	0.074	0.53	0.369
Methanol	0.61	0.071	0.77	0.544
Water	1.13	0.23	3.3	1.000
Ethanol	0.71	0.16	1.2	1.074
Propanol	0.76	0.27	11	1.945
Butanol	0.69	0.31	3.1	2.544
Pentanol	0.83	0.26	4.3	3.619
Decanol	1.20	0.19	65	10.60
Ethylene glycol	0.54	0.20	4.6	16.10

[a] Uncertainties are obtained from non-linear least-squares analysis, in some cases from several sets of measurements. The uncertainties are typically 10% for τ_1 and somewhat larger for τ_2. With the exception of acetonitrile and methanol, the value of τ_2 is of the order of or longer than the time range of the experiment. An uncertainty of 60% results for decanol.
[b] Values from the *CRC Handbook of Chemistry and Physics*, 74th edition.

* In deliberate 'slow-flow' experiments in a flowing sample cell, where the high repetition rate laser pulses interogate the same sample volume many times, the accumulation of a photoproduct is indeed possible. We have observed that the negative-time signals in slow-flow experiments are negative in amplitude, indicating a net absorption of the probe. This absorption, presumably from the photoisomer, is still dominated by a positive bleach/stimulated emission response at positive time. The high flow rate experimental results reported here (cf. Fig. 3) always show a negative-time signal that is zero in amplitude, indicating the absence of any detectable photoproduct accumulation from previous laser pulses (i.e. $\geq$ 13 ns prior).

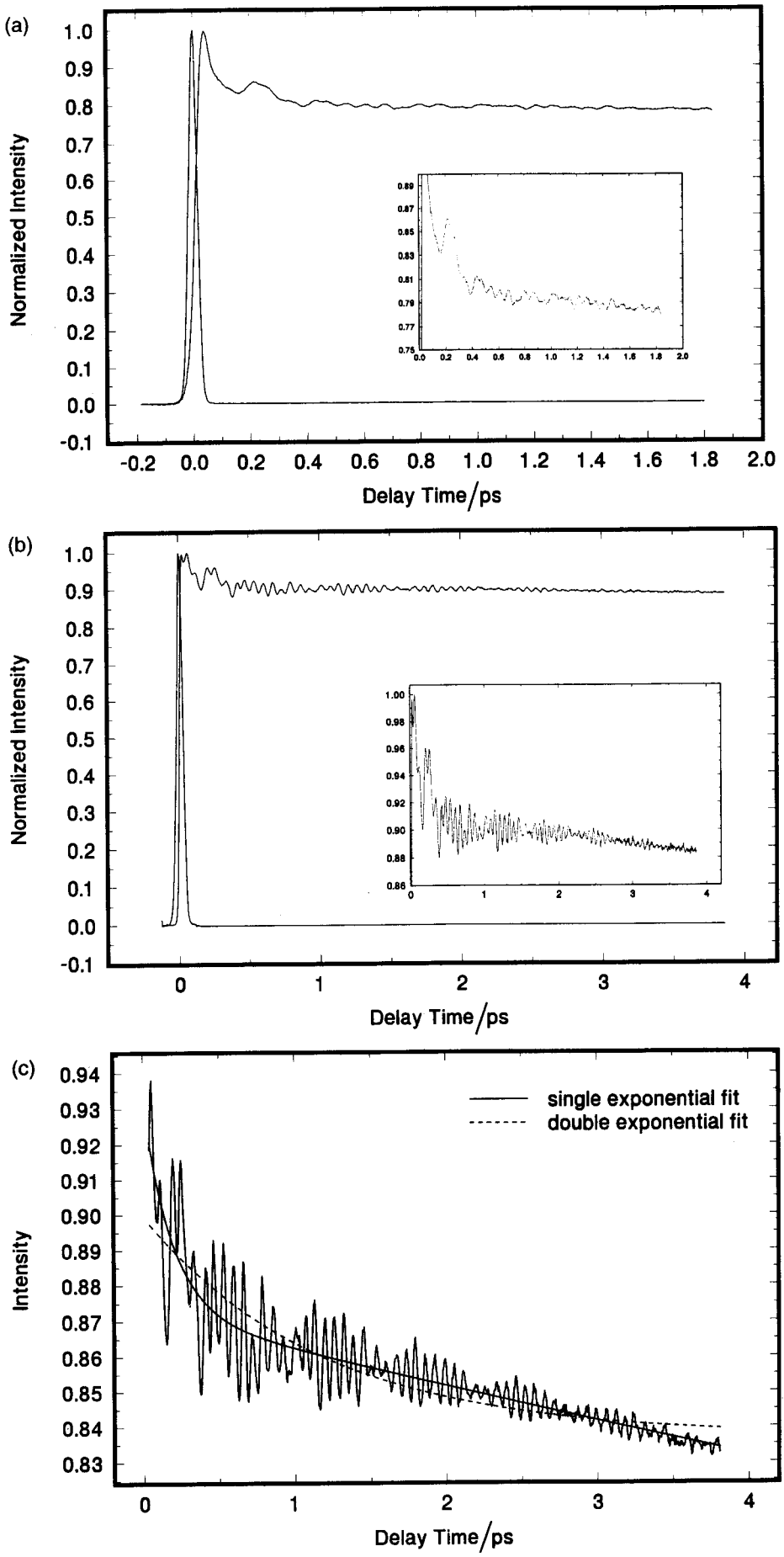

Figure 3. (a) Pump–probe signal of HITCI in ethylene glycol using 35 fs pulses; (b) pump–probe signal of HITCI in ethylene glycol using 20 fs pulses; (c) pump–probe signal of HITCI in *n*-decanol using 20 fs pulses. The data points are connected by a thin solid line. The heavy lines through the data are single (solid) and double exponential (dashed) plus offset fits to the data.

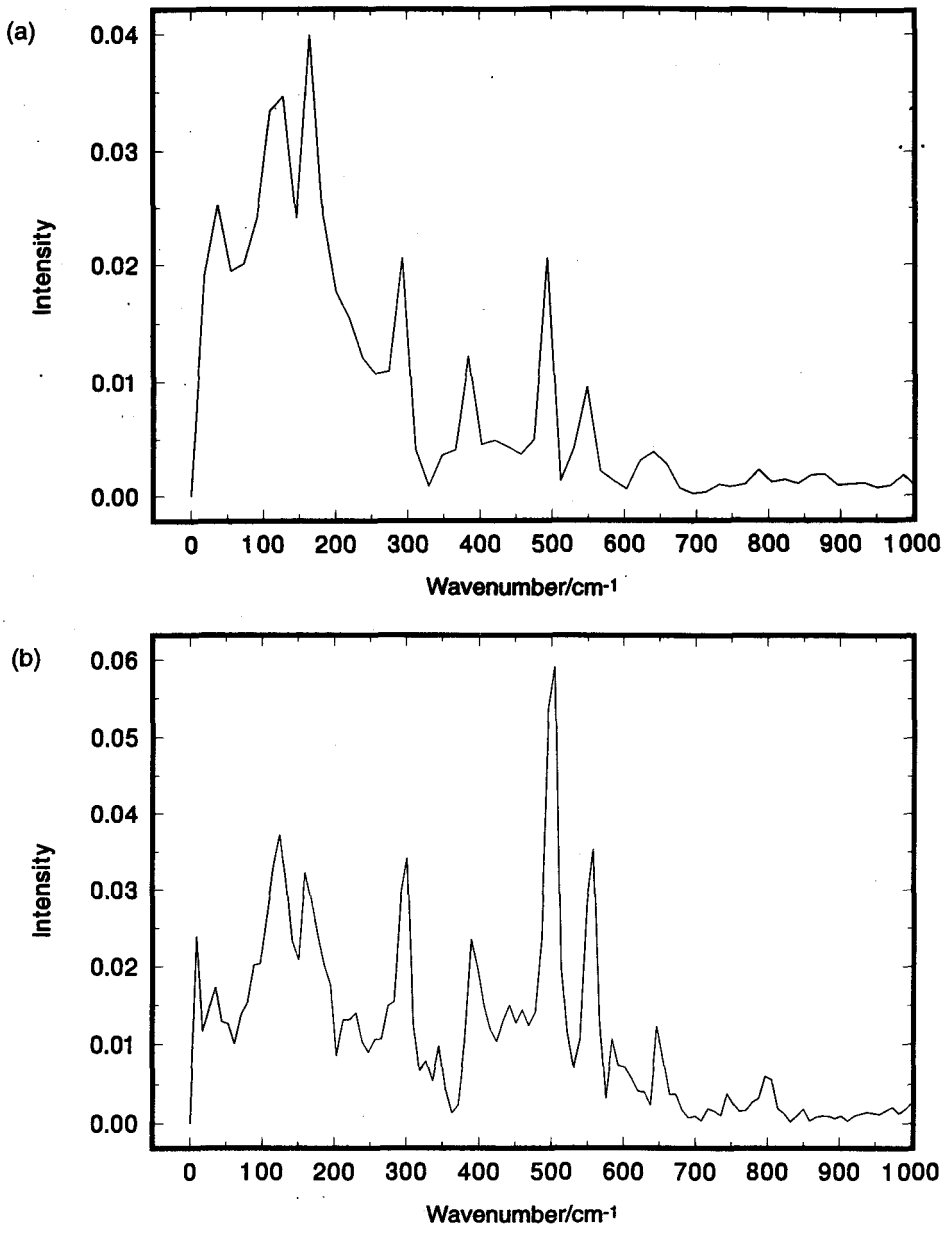

Figure 4. (a) Fourier spectrum of the pump–probe signal displayed in Fig. 3(a). (b) Fourier spectrum of the pump–probe signal shown in Fig. 3(b).

in the analysis described below remain un-normalized with respect to the pump–probe response function. The Fourier transformed results (i.e. spectra) are, however, normalized (i.e. deconvoluted in the wavenumber domain) to the system response function, that is, the pump–probe intensity autocorrelation.

Figure 5 shows the oscillatory portion of the data from Fig. 3(c) of HITCI in decanol with the exponential and offset components removed. The solid line through the data points is from the LPSVD analysis, which is performed with the assumption that the experimental data can be represented by a sum of exponentially damped cosinusoidal functions:

$$S_{pp}(t_d) = \sum_i A_i \cos(\omega_i t_d + \phi_i)\exp(-t_d/\tau_i) \qquad (1)$$

where ω_i is a vibrational wavenumber difference in either electronic state. Density matrix descriptions of non-linear spectroscopy[11,16] and time domain measurements[9–11] have established that this functional form is appropriate for underdamped vibrational coherence. The fit to the data for pump–probe time delays, t_d, beginning at 40 fs delay time is excellent. The very high quality of the data allows the simultaneous elucidation of the wavenumber and relaxation times, τ_i, of many oscillatory modes. This analysis identifies eight damped oscillatory components for HITCI in all of the solvents. All Bohr wavenumbers agree with the peaks observed in the absolute magnitude spectrum. The fitting parameters for decanol are summarized in Table 2. The oscillatory components, some of which are identified with energies of ground-state fundamentals, show a range of damping times. The highest wavenumber modes have the longest damping time while the lowest wavenumber modes have the shortest damping times. Since rotational reorientation and other electronic relaxations are

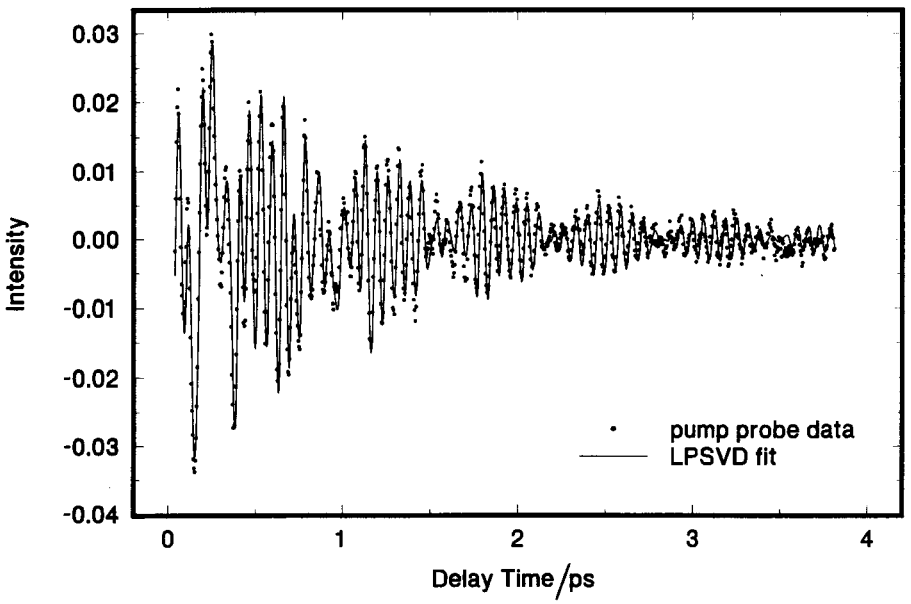

Figure 5. Pump–probe signal of HITCI in *n*-decanol after subtracting a fit to a double exponential plus offset. Eight components are obtained from the LPSVD analysis that gives the fit. The parameters are summarized in Table 2. The solid line represents the corresponding sum of eight damped cosine functions.

slow compared with the decay of vibrational coherence, the damping constants are the vibrational dephasing times.

Vibrational coherence in various solvents

Pump–probe measurements were performed in a variety of solvents including alcohols (methanol through pentanol and decanol), water, ethylene glycol and acetonitrile. The time constants for the decay of the lowest six of the eight wavenumber components identified in HITCI are presented in Fig. 6. The data are plotted against the viscosity of each solvent; the symbols correspond to the different vibrational wavenumbers (see the figure caption). The time constants for vibrational dephasing are well separated and increase monotonically with vibrational wavenumber. This trend is most clearly seen in the solvents of greater viscosity. The scatter in the time constants for the solvents of smaller viscosity may reflect solvent-dependent relaxations or possible solvent-dependent shifts of the absorption and emission bands. The pump–probe signals for the less viscous solvents (i.e. acetonitrile, methanol and ethanol) are also noisier owing to dye jet instabilities. The resultant greater uncertainty in the determined relaxation rates may also contribute to the scatter in the time constants. Since there is no apparent solvent dependence of the vibrational dephasing for any of the detected wavenumber components, we calculate solvent-averaged time constants (using the longer chain alcohols and ethylene glycol data) as indicated by the horizontal lines.

Table 2. LPSVD fitting parameters for HITCI in decanol[a]

wavenumber/cm^{-1}	Time constant/ps[a]	Phase/°[b]	Amplitude[c]
118	0.69	32	0.0056
161	0.47	70	0.0052
295	0.68	27	0.0054
390	0.85	23	0.0036
501	1.44	5	0.0084
554	1.54	22	0.0052
647	0.82	12	0.0030
798	1.14	40	0.0013

[a] Error in time constant is typically 5%.
[b] Accuracy of phase angle is typically 20°.
[c] Total signal level normalized to 1.

The experimental rate for the decay of vibrational coherence is most generally interpreted as the inverse of the total dephasing time, $1/T_2$. In the case of a Markovian bath, the total dephasing rate can be expressed in terms of a rate describing population relaxation, $1/T_1$, and a pure dephasing rate, $1/T_2^*$. Oxtoby and Rice have formulated a quantum mechanical description of the population relaxation contribution to total vibrational dephasing for an oscillator coupled to a phonon bath.[32,33] They have shown that the population relaxation is given by

$$\tau_{\text{vib.}}^{-1} \propto \exp[-c\omega_{\text{vib}}/\omega_0] \qquad (2)$$

where ω_0 is a characteristic phonon wavenumber of 50–100 cm^{-1} and c is a constant of order unity. Further, an exponential dependence for the rate of vibrational population relaxation with oscillator wavenumber is also obtained from the isolated binary collision model.[34] In both cases the magnitude of the constant c in the exponent is expected to be of the order of unity when the oscillator wavenumber ω_{vib} is scaled by 100 cm^{-1}.

The pronounced dependence of the vibrational dephasing rate of HITCI on the oscillator wavenumber is clearly demonstrated in Fig. 7; the solvent-averaged rate of dephasing decreases by a factor of four for vibrational wavenumbers ranging from 120–550 cm^{-1}. The solid curve in Fig. 7 is a fit of Eqn (2) to the six lowest

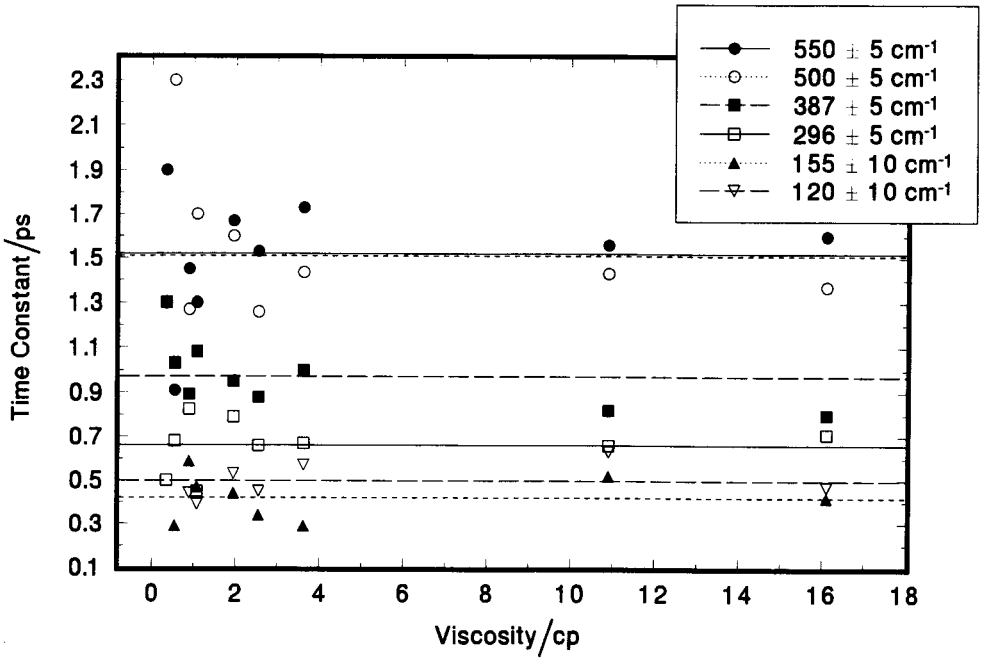

Figure 6. Time constants as a function of solvent viscosity for different wavenumber vibrational coherence contributions. The legend indicates symbols associated with the individual wavenumber modes. The horizontal lines through the points are the solvent-averaged decay times for each mode.

wavenumber components. The quality of the model fit is very good. Moreover, the exponent of the fitted curve has a value of 0.3, which is in close agreement with the theoretical treatment. Further discussion about the good comparison between the vibrational dephasing data and Eqn (2) is given in the next section.

The trend in the rate of vibrational dephasing vs wavenumber of the vibrational oscillator is not simply a function of this one chromophore. The measured rates of vibrational dephasing for a similar cyanine dye, HDITC perchlorate (1,1',3,3',3'-hexamethyl-4,4',5,5'-dibenzo-2,2'-indotricarbocyanine) are superimposed on the same graph (open square symbol). The solvent-averaged rate of vibrational dephasing in HDITCP is calculated from only two solvents, butanol and ethylene glycol. The data points are well fitted by the same curve fitted to the HITCI data. This agreement suggests that the rate of vibrational dephasing is more dependent on the oscillator wavenumber as opposed to the specific chromophore.

Wavelength-resolved pump–probe signals

The transmitted probe spectrum was dispersed and resolved at discrete wavelengths and the transient

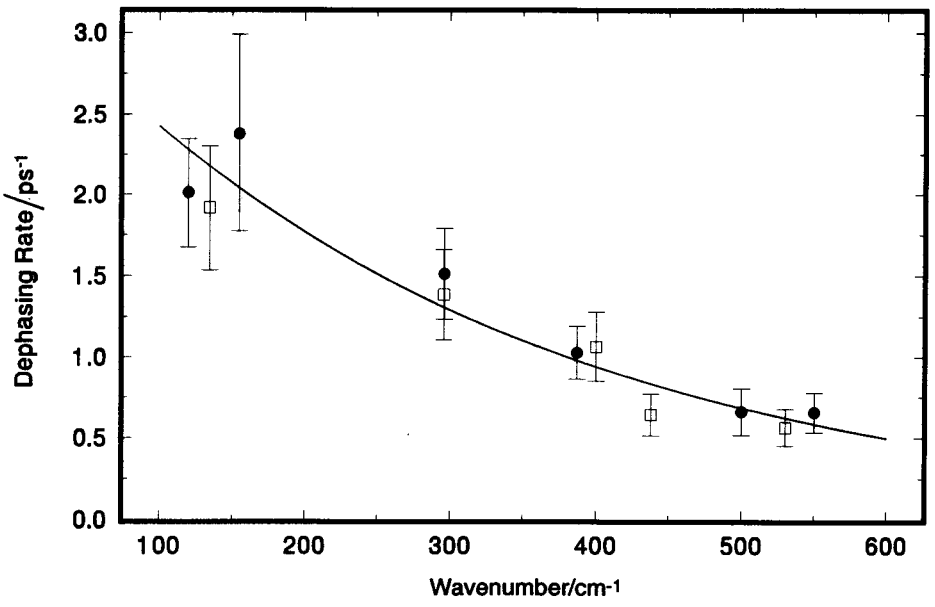

Figure 7. Solvent-averaged dephasing rates versus oscillator wavenumber. Exponential fit to points with wavenumber < 600 cm^{-1}. Fit: $k = 3.39 \exp(-0.0031\omega)$. Only the first six wavenumbers are fitted since the amplitudes of the 650 and 800 cm^{-1} modes are only 4–5 times greater than the noise as judged from the Fourier spectra. As a result, the fitting gives shortened decay times.

response was recorded as a function of pump–probe delay time. The full three-dimensional signal, $P^{(3)}(t, \lambda)$ of HITCI in propanol shown in Fig. 8 bifurcates into absorption and emission bands within 2 ps. The near zero-of-time pump–probe spectrum is similar to the absorption spectrum. Vibrational coherence features are seen from early times and oscillate from blue to read and back. The amplitude of the 'red' spectral features are seen to grow in while the 'blue' spectral features decline. This spectral evolution results in the growth of the red band which is associated with the steady-state emission spectrum. Simulation of these wavelength-resolved pump–probe transients by the non-linear response function method[3] will be reported elsewhere.[35] However, analysis of the spectral features associated with the absorption and emission maxima are useful for elucidation of the underlying cause for spectral evolution.

Figure 9(a) and (b) show two wavelength components of the spectral evolution of the pump–probe signal that exemplify the temporal behavior in the $S_0 \rightarrow S_1$ Franck–Condon region (i.e. 750 nm) and from $S_1 \rightarrow S_0$ stimulated emission (i.e. 790 nm). The former curve shows a decay while the latter exhibits build-up dynamics followed by a decay. The amplitudes of these curves are normalized to the pump–probe signal intensity at 1.7 ps time delay. The 750 nm curve is fitted with an exponential decay plus offset while the 790 nm curve is fitted with one rising exponential component plus an offset. The time constants for the fast decay at 750 nm (i.e. 390 ± 20 fs) and exponential rise at 790 nm (i.e. 360 ± 30 fs) are nearly the same. Figure 9(c) shows the wavelength integrated pump–probe signal of HITCI in propanol. This figure also shows a biexponential plus offset fit superimposed on the experimental data; the fitted curve has a fast exponential relaxation time constant of 250 ± 20 fs. The faster dynamics for the wavelength integrated scan and more pronounced biexponential decay result from the range of build-up and decay contributions from different wavelength components.[35]

The inset to each panel in Fig. 9 is the absolute magnitude spectrum of the respective temporal data set. It should be noted that the waveform in Fig. 9(a) predominantly shows the low-wavenumber modes. Comparison of the oscillatory dynamics detected at 750 and 790 nm indicates that several of the lowest wavenumber components arise from a coordinate-dependent sensitivity to the vibrational wavepacket motion on the S_1 potential energy surface. The low-wavenumber features at 120 and 160 cm^{-1} contribute to the prominent feature at 0.2 ps delay time in Fig. 9(a) and (b). The oscillatory contribution in the two figures is, however, of opposite sign, that is π-phase shifted. (The signs of the Fourier components are not reflected in the absolute magnitude spectra shown as insets in the two figures.) The fact that these components are of opposite sign suggests that they are probed by a stimulated emission process from S_1 but from opposite turning point regions.[16,35] From the aforementioned observations and from the results of wavepacket simulations,[35] we interpret the low wavenumber (120, 160 cm^{-1}) features as primarily arising from the S_1 state whereas the high-wavenumber features arise primarily from S_0. The 750 nm detection wavelength primarily probes S_1 vibrational dynamics. Detection at 790 nm yields high-wavenumber components that agree with known ground-state vibrations.[31] Of course, because four pathways contribute to pump–probe signals for a two-electronic level system,[16b] assigning spectral features to one electronic state or the other is not unique. However, simulations do show propensities for S_0 or S_1 contributions to the total jump–probe signal at different wavelengths.[35]

Wavepacket probing via the $S_1 \rightarrow S_n$ transient absorption would be expected to give features of opposite sign to those shown. In analogy with the phase

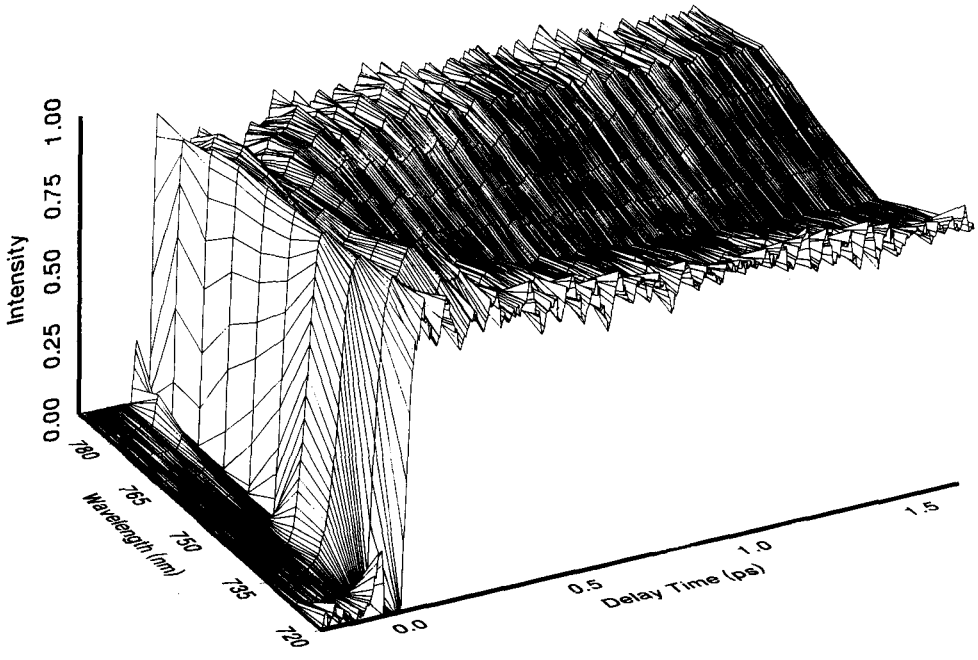

Figure 8. Wavelength and time-resolved pump–probe signal of HITCI in propanol. The monochromator resolution is 2 nm and scans are recorded at 10 nm intervals. The maximum of each scan was normalized to 1.

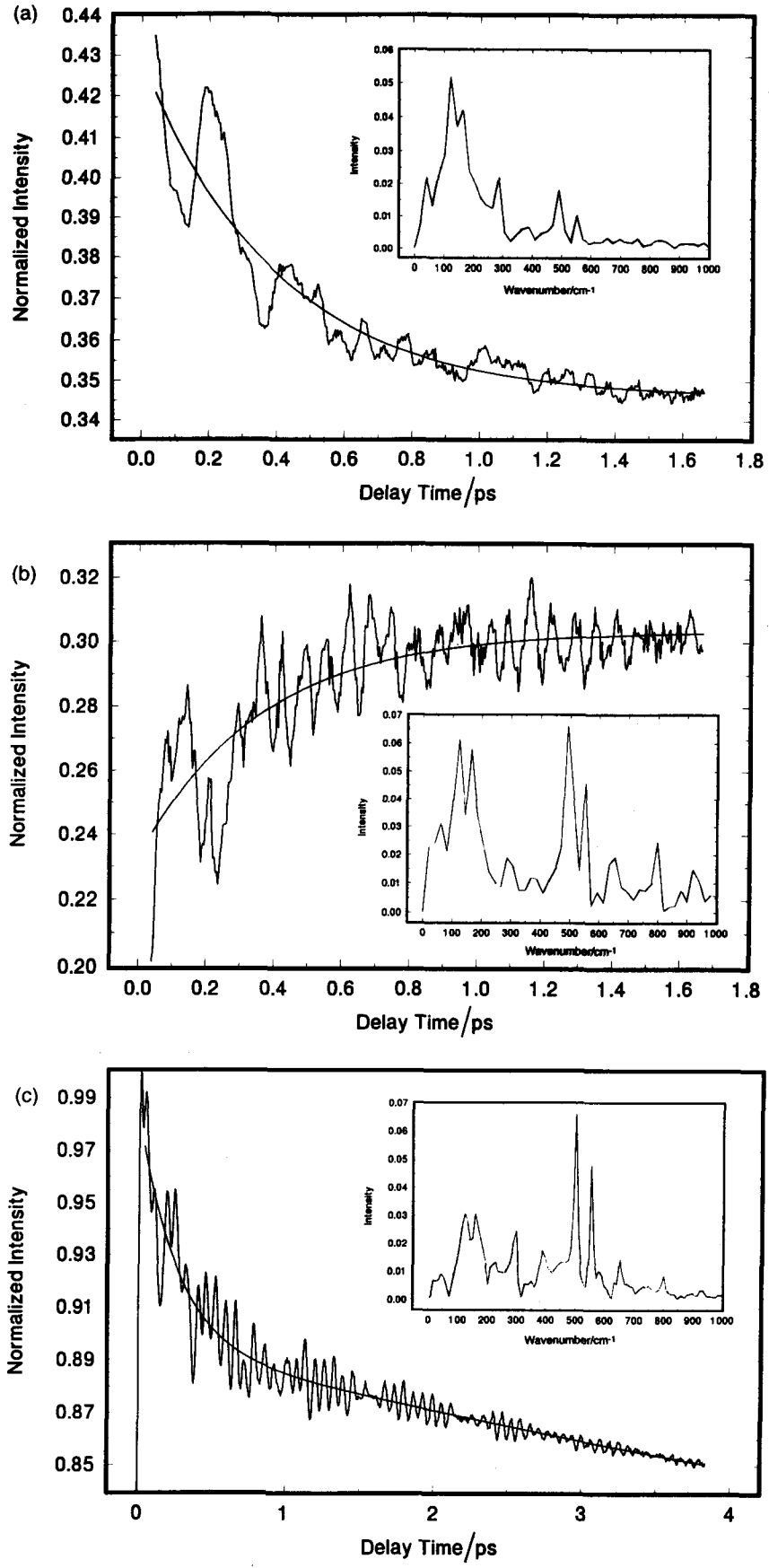

Figure 9. (a) Wavelength-resolved pump–probe signal of HITCI in *n*-propanol at 750 nm. Single exponential fit plus offset. Fit: $y = 0.346 + 0.083 \exp(-t/0.39)$; uncertainty of time constant is 0.02. Inset is the Fourier spectrum of the time domain data. (b) Wavelength-resolved pump–probe signal of HITCI in *n*-propanol at 790 nm. Single exponential fit plus offset. Fit: $y = 0.303 - 0.071 \exp(-t/0.36)$. Inset is the Fourier spectrum. In both cases the error in the time constant is approximately 7%. (c) Wavelength-integrated pump–probe signal of HITCI in *n*-propanol (note the change in time range). The signal is normalized to a peak value of 1. Solid line is double exponential plus offset. Fit: $y = 0.715 + 0.0917 \exp(-t/0.254) + 0.180 \exp(-t/11.36)$, and the error is about 5%. Inset: Fourier spectrum.

angle for excited state wavepacket motion in molecular iodine,[8] the 750 nm probe feature would give a minus cosine waveform if probed via $S_1 \rightarrow S_n$ absorption whereas a plus cosine result is observed. Further, if the major contribution to the signal were an absorption, the intensity as plotted in these figures would be negative not positive (see earlier footnote). Therefore, the contributions to the signal arise from $S_0 \leftrightarrow S_1$ absorptive or emissive transitions and do not have significant contributions from assumed $S_1 \rightarrow S_n$ transient absorptions.[26,28] The other wavelength-resolved scans also do not show absorptive features on these time-scales.

Solvent-dependent overdamped dynamics

Two interpretations of the decay and build-up dynamics observed in Figs 8 and 9 can be rationalized: (i) solvation of the S_1 state by the dipolar solvent with a resulting red-shifting of the emission spectrum or (ii) population relaxation of overdamped low-wavenumber vibrational modes in each electronic state. In the first case the (Gibbs free) energy of the excited electronic state is reduced with respect to the ground state owing to rearrangement of the dipolar solvent (i.e. solvation). In the case of solvation, only the emission spectrum would be expected to exhibit a time-dependent wavenumber shift. The latter case of population relaxation with the excitation detuned from the absorption maximum would produce time-evolving absorption and emission spectra that shift to higher and lower energies, respectively, and narrow with time. Examination of the steady-state Stokes shift in a range of solvents can be used to determine whether the relaxation results from solvation.

The steady-state solvent-dependent Stokes shifts, the energy difference between the absorption and emission 0–0 transitions, assumed to be the absorption and emission maxima, were measured in the aforementioned solvents and also CH_2Cl_2, CH_3Cl, CCl_4, DMSO, octanol, chlorobenzene, benzene and toluene. The change in the dipole moment of the solute on optical excitation can be obtained from the relation given by Ooshika, Lippert and Mataga (OLM):[36]

$$\langle \Delta\nu \rangle = \langle \Delta\nu_a \rangle - \langle \Delta\nu_f \rangle = \frac{2(\mu_e - \mu_g)^2}{ha^3}\left(\frac{\varepsilon_0 - 1}{2\varepsilon_0 + 1} - \frac{n^2 - 1}{2n^2 + 1}\right) \quad (3)$$

where $\langle \Delta\nu_j \rangle$ are average shifts in the absorption and emission transitions. Figure 10 is a plot of Stokes shift vs the polarity parameter given in the final parentheses on the right-hand side of Eqn (3). The straight line in the figure is a fit to all of the points excluding the solvents in the box, which are benzene, toluene and CCl_4 (analysis of the absorption and emission spectra relative to the other polar solvents indicates that these three solvents cause the HITCI chromophore to form aggregates; the chromophore is only slightly soluble in these solvents, and these data are, therefore, not suitable for inclusion in the analysis). The small magnitude of the Stokes shift compared with, for example, coumarin dyes[37] and the small, almost zero, slope for the fitted line indicates that the change in dipole moment on optical excitation is less than 1 D. This result is in agreement with recent *ab initio* electronic structure calculations, which predict only a small change in charge distribution upon optical excitation from S_0 to S_1 in this type of cyanine dye.[38]

Further, we examined the Stokes shift for different excitation wavelengths and found that the shift goes to zero for excitation at the peak of the emission spectrum. This further indicates that relaxation by solvation is small for HITCI and that the Stokes shift probably arises from $S_0(v = 0) \rightarrow S_1(v = n;\ n \geq 1)$ excitation and

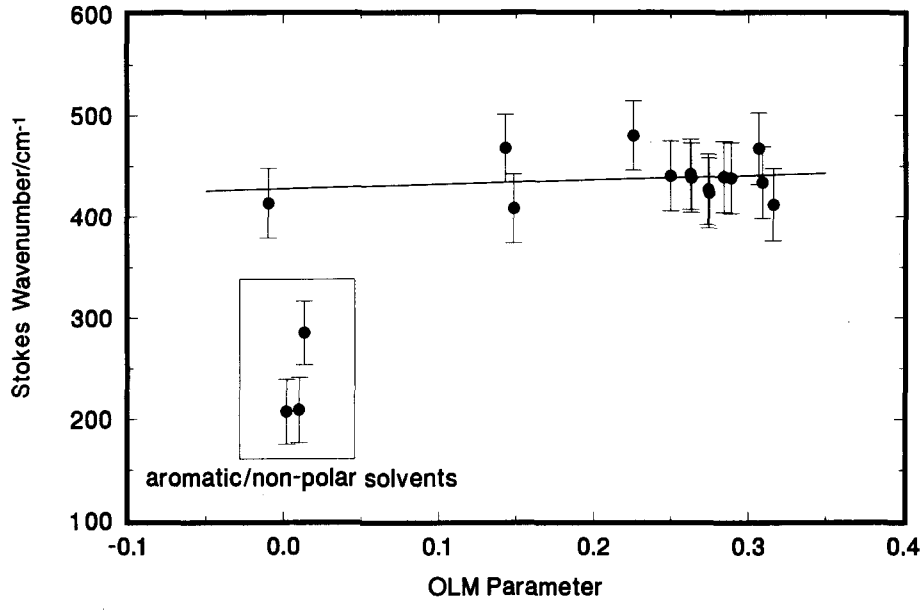

Figure 10. Stokes-shift vs OLM parameter. Line is least-squares linear fit through all points accept those inside box. The non-zero intercept results from not having subtracted the gas phase 0–0 absorption and emission transitions. The fluorescence emission peak position was obtained in a series of increasingly dilute solutions and extrapolated to infinite dilution. It should be noted that the wavelength of the emission peak remained constant for excitation at and to the red of the peak absorption wavelength up to the value of the emission maximum.

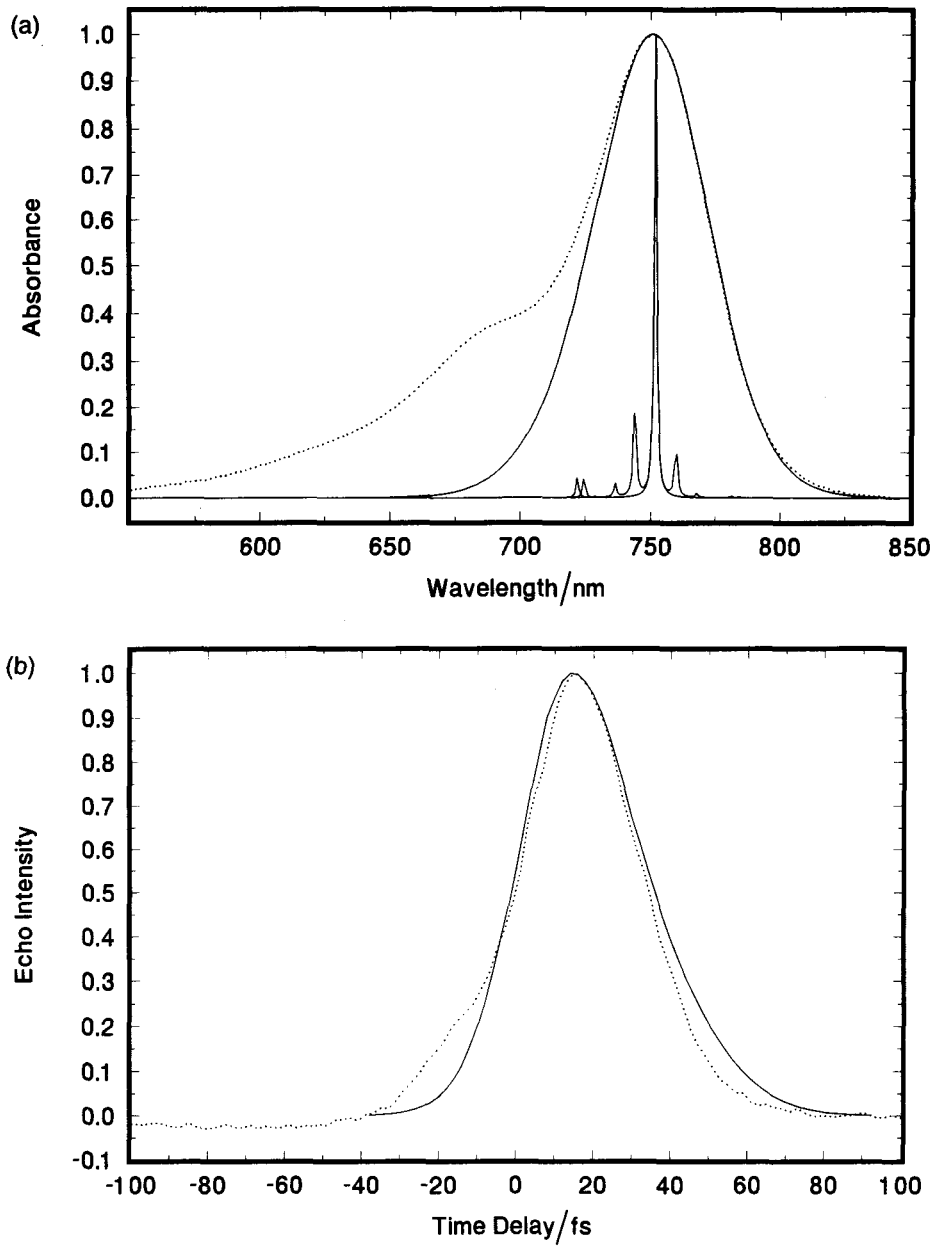

Figure 11. Multi-mode calculations for HITCI–DMSO. (a) Measured (dotted line) and optical dephasing simulation (solid line) of steady-state absorption spectrum using the following intra-chromophore modes and displacements: $\omega = 500$ cm^{-1}, $D = 0.3$; $\omega = 550$ cm^{-1}, $D = 0.3$; and $\omega = 140$ cm^{-1}, $D = 0.5$. (b) Measured (dotted line) and optical dephasing simulation (solid line) of two-pulse echo using same parameters as absorption spectrum.

$S_1(v = 0) \rightarrow S_0(v = n;\ n \geq 1)$ emission. Such transitions imply that the surfaces are displaced with respect to each other, resulting in Franck–Condon vibrational progressions building off of the 0–0. Such progressions facilitate preparation of vibrational wavepackets along the displaced coordinates by impulsive excitation and the population of vibrationally excited levels.

Finally, the results of fitting the pump–probe data in different solvents, summarized in Table 1, are useful for understanding the processes giving rise to relaxation and spectral evolution. The focus is on the rapid exponential decay term obtained from biexponential fitting. This decay component, designated as τ_1 in Table 1, exhibits a significant solvent dependence that may be due to population relaxation of the underdamped vibrational modes described above or to the overdamped response of low-wavenumber modes of the molecule. Pump–probe responses have contributions from both diagonal and off-diagonal elements of the density matrix; here these elements describe the vibrational states of HITCI. If it is assumed that the vibrational coherence features, which are described by the off-diagonal elements, decay by population relaxation, then simple addition of the relaxation rates of the underdamped modes (120–800 cm^{-1}) with consideration of their amplitudes would give the corresponding population decay rate. Examination of the vibrational coherence dephasing times given in Fig. 6, however, does not yield the solvent dependence summarized in Table 2.

A second explanation, which invokes the contribution of overdamped chromophore motions to the pump–probe signal, implies that very low-wavenumber vibrational modes exist in HITCI which are rapidly damped by solvent fluctuations. The lowest wavenumber under-

damped mode that can be assigned a wavenumber is at 120 cm^{-1}. It is certainly true that lower wavenumber modes that undergo large amplitude motions exist in these cyanine dyes. Clearly the wavenumber of these vibrational modes cannot be established in the present experiments, so an analysis of the solvent-dependent relaxation of such low-wavenumber motions must focus on the properties of and coupling to the solvent.

Role of intra-chromophore modes in photon echo spectroscopy

Optical coherence measurements, including photon echo spectroscopy, are a sensitive measure of solvent interaction with the optical (electronic) coordinate of the chromophore.[3,12b,18,20] Simulation of such third-order polarization responses provide a way of establishing the spectrum of solvent fluctuations that cause changes in the S_0–S_1 electronic energy difference in, for example, HITCI.[20,39] In other work,[20] we have established an approach for relating the dephasing spectral density to the polarizability spectral density of the pure solvents. Further simulations of two-pulse, three-pulse and time-gated echo data[40] indicate the necessity for including intra-chromophore vibrational modes in the analysis[41] [a 1300 cm^{-1} mode due to backbone bending near 1300 cm^{-1} (not shown in Fig. 11) also has a significant displacement of 0.3, accounting for the high-energy shoulder in the absorption spectrum; this mode is not impulsively driven in the experiments reported here but still contributes to the total Stokes shift]. Vibrational displacements are obtained by simulation of pump–probe data, as presented above, including the three most prominent modes in the absolute magnitude spectra (i.e. 140, 500 and 550 cm^{-1}, where the first is the average wavenumber of the 120 and 160 cm^{-1} modes described above).

Figure 11(a) shows the steady-state absorption spectrum of HITCI in DMSO. Also shown is an optical dephasing simulation[41] of the absorption spectrum using several intra-chromophore modes (see figure caption). Figure 11(b) shows a simulation of a two-pulse photon echo of HITCI in DMSO using the same parameters as the absorption spectrum. These simulations confirm that intra-chromophore modes with the stated displacements (see figure caption) can account for 90% of the measured steady-state Stokes shift.[41] This finding supports the idea that the observed Stokes shift is due to intra-chromophore displacements and relaxation and not to solvation. More detailed results of these simulations will be presented elsewhere.[41]

DISCUSSION

Frequency-dependent friction and vibrational dephasing

Microscopic friction originates in the coupling of solvent fluctuations to the chromophore dynamics along the solvation of reaction coordinate.[1] For this reason, the dynamics of chemical processes are expected to depend on the frequency response of the solvent. It has been shown that the damping constant for vibrational population relaxation in CH_3Cl is related to the friction in the form of the amplitude of the solvent spectral density at the oscillator frequency.[42]

Contributions of the finite frequency response of the surrounding bath to the dynamics of chemical reactions such as unimolecular barrier crossing processes have traditionally been discussed in terms of the generalized Langevin equation (GLE). The friction that enters this equation is proportional to the time correlation function of the fluctuating forces that hinder the particles' motion over the potential barrier.[43] Experimental determined rate coefficients determined as a function of the solvent shear viscosity for the photoisomerization of *trans*-stilbene exhibit marked deviations from predictions given by Kramers theory in the Markovian limit.[44] However, the viscosity dependence of the experimental rates could be satisfactorily described by incorporating a time-dependent frictional drag as proposed by Grote and Hynes.[45] On the other hand, extensive studies of the pressure dependence of this reaction for a variety of different solvents show that this model system (stilbene isomerization) is not sufficiently sensitive to establish any influence of a memory kernel describing the friction; the experimental rates can be remarkably well represented with a deltacorrelated friction coefficient.[46] In order to test experimentally the validity of GLE-based theories, it is important to choose model systems that are characterized by rate coefficients which are on the order of the inverse decay time of the correlation functions relevant to the reactive motion. Apparently, this condition is not fulfilled for the reaction systems investigated so far, even for relaxation processes on barrierless potentials which can occur on time-scales significantly below 1 ps.[47]

In the present study, we examined another type of frequency (or wavenumber)-dependent 'friction.' It was shown in Fig. 7 that the relationship between the damping constant and oscillator wavenumber yields a monotonic trend. Further, Fig. 7 shows that the vibrational dephasing rate is inversely proportional to the exponential of the oscillator wavenumber, indicating that the high-wavenumber motions are less rapidly damped.* This trend is similar to the wavenumber-dependent friction predicted for chemical reactions where high-wavenumber motions on sharp barriers are damped less rapidly than low-wavenumber motions.[48,49] For isomerization this trend is intuitively clear, the solvent can respond adiabatically to the slow solute motions and strongly hinder the motion, whereas the solvent cannot respond quickly to rapid solute motions.

The result from the fitted curve in Fig. 7, that the vibrational dephasing appears to be primarily due to population relaxation, is unexpected in that it is conventionally believed that vibrational pure dephasing is

* We have performed semi-empirical (MNDO, Spartan) electronic structure calculations on HITCI to examine the types of motions associated with the low frequency vibrations. Generally, these were found to be torsional or rocking motions suggesting the connection with barrier crossing. Torsional isomerization is the process involved in creating the photoisomer of HITCI and has been well studied in shorter cyanine dyes such as DODCI, where the isomerization occurs of the order of 100 ps.

more rapid than population relaxation. Dominant population relaxation is possible in a situation where the correlation function that describes solvent-induced vibrational pure dephasing is the same for the different levels that are coherently prepared for each mode. In this way, the solvent fluctuations would shift all vibrational energies of a given mode within a given molecule by the same amount. This implies linear coupling of the bath to harmonic modes of the molecule, and population relaxation would involve energy loss to the bath or excitation to higher energy levels by the bath. More efficient energy transfer and therefore a faster rate for population relaxation at smaller vibrational level spacing would result. Harris and co-workers[50] have shown that population relaxation of molecular iodine in solution is much faster in the high energy part of the X-state vibrational mainfold than near the bottom of the potential. Conclusive proof that the rate of vibrational coherence relaxation observed here is due to population relaxation as opposed to vibrational pure dephasing would require a more selective probing method.[51]

It is more likely that the observed wavenumber dependence for vibrational dephasing is due to pure dephasing since vibrational pure dephasing in large molecules also tends to decrease with increasing oscillator wavenumber.[19] This dephasing mechanism would have a $1/\omega^2$ dependence; this functional form also fits the experimental data in Fig. 7 fairly well, although with a slightly porrer correlation coefficient. Oxtoby[19a] and Battaglia and Madden[52] have shown that inclusion of solute vibrational anharmonicity creates a favorable mechanism for solute–solvent coupling. This requires a second-order coupling that is still more significant, by an order of magnitude or more, than the linear coupling referred to above. Vibrational pure dephasing occurring by this kind of mechanism and would then be the dominant contribution to the observed total dephasing. This would also account for a slower rate of vibrational dephasing for larger vibrational wavenumbers since the anharmonicity would be less significant and fewer bath modes.

Tucker and co-workers[53] have shown that a typical model of a reactive solute in condensed media in a weak damping regime exhibits two types of slow solute energy relaxation controlled by different wavenumber ranges of the solvent's spectral profile. The initial relaxation pathway is controlled by the interaction of low-wavenumber solvent modes with the solute's unbound motion. This relaxation is followed by a secondary mechanism, conventional vibrational energy relaxation, that is controlled by the interaction of the high-wavenumber solvent modes with the vibrational motion of the solute. Another possibility for a bath that can cause vibrational dephasing are the low-wavenumber overdamped modes of the chromophore itself. The intra-chromophore vibrational coupling would be largely solvent independent and could account for the lack of solvent dependence for the underdamped modes. Coupling to this intramolecular 'bath' depends strongly on the anharmonicity of the mode. Basically, the high-wavenumber less anharmonic vibrational modes 'tune out' of the spectrum of bath modes with large occupation and amplitude and, therefore, dephase less rapidly.

Relaxation in pump–probe measurements: solvation

Solvation is the process of solvent reorganization in response to a change in chromophore electrostatic charge distribution that acts to minimize the free energy of the chromophore–solvent system.[37] The time evolution of the process has been studied by examining the time dependent fluorescence Stokes shift of the chromophore emission.[54] The fluorescence emission from electronically excited molecules with larger dipole moments than in the ground state red shifts in time in the presence of a dipolar solvent. The cause–effect relationship of chromophore and solvent interaction can be understood through a reaction field description of the correlation function for solvation and spectral evolution.[55,56] The solvent motions involved in reconfiguration have been studied in molecular dynamics simulations.[57,58] Experimentally measured solvation times are certainly faster than longitudinal relaxation times.[37,54] High time resolution measurements allowed the detection of inertial contributions to the solvation response occurring on 50–200 fs time-scales.[59] These time-scales are similar to the fast relaxation component observed here for the prompt exponential component.

However, there are several reasons for assuming that solvation is not the principle cause of the observed overdamped relaxation. The very small slope of the plot of Stokes shift vs the OLM relation [Eqn (3)] shown in Fig. 10 indicates that the change in dipole moment of the HITCI chromophore upon optical excitation is significantly less than 1 D for a broad range of solvents. Electronic structure calculations done for symmetric cyanine dyes also show little change in charge density for $S_0 \rightarrow S_1$ excitation. Simulations of two-pulse photon echos and linear absorption spectra show that 90% of the measured steady-state Stokes shift can be accounted for by intra-chromophore modes.[41] Further, Maroncelli *et al.*[60] have recently derived a simple expression for the inertial solvation response which is the product of the dipole density and the average squared rotational wavenumber. It is found that the fast relaxation data listed in Table 1 do not correlate with this parameter.

Exponential relaxation in pump–probe measurements: population decay

The aforementioned results indicate that solvation is not the dominant mechanism causing exponential relaxation of the total probe-pulse energy. The results of our exponential data fitting can be compared with previous time-resolved studies of vibrational population relaxation in S_1 of Nile Blue and Oxazine 725 in methanol.[61] These earlier studies were performed with 70 fs pulses and established relaxation times of 400–500 fs for these other dyes in methanol. A single exponential fit to the HITCI–methanol data yields 600 fs for the relaxation time, in good agreement with the previous work. This favorable comparison with previous studies further suggests that the exponential relaxations observed here for HITCI reflect solvent dynamics that influence population relaxation.

The shear viscosity in the Markovian limit is directly related to friction[62] as applied to unimolecular barrier crossing processes in solution and scales linearly with

the collision frequency.[63] The rate constant of this type of reaction is expected to scale inversely with viscosity. The correlation of the rate with the inverse of the viscosity is well established for isomerization reactions in high-pressure gases and liquids.[46,64,65] Figure 12 is a log–log plot of the fast relaxation rate, obtained from a biexponential fit of the pump–probe data against the solvent viscosity. The fitted line is for all the pump–probe signals except decanol and ethylene glycol. Figure 12 shows that increased viscosity, and hence friction, results in slower exponential relaxation. The slope of -0.68 for the line in Fig. 12 is in agreement with the relationship[46]

$$k \propto \eta^{-\alpha} \tag{4}$$

where $0 < \alpha < 1$. It appears that the overdamped component to the pump–probe signal and the significant solvent dependence results from the coupling of fast solvent motions to low wavenumber (i.e. < 100 cm^{-1}) overdamped vibrations of HITCI. The mechanism of the coupling is not known, although the trend of the fast relaxation scales inversely with viscosity. This behavior is similar to that observed for unimolecular reaction dynamics in dense media.[46]

Deviations from the linear trend at high viscosity probably result from the increasing contribution of the decaying wavelength-resolved components to the total signal. This increased decay component comes about from the linear shift of the absorption maximum to longer wavelengths, which is most pronounced for the high-viscosity solvents decanol and ethylene glycol. This shift of the absorption maximum, with an essentially constant Stokes shift, would increase the spectral overlap of the laser pulses with the absorption band.

Influence of sequence band transitions

All of the low-wavenumber vibrational modes of HITCI are thermally populated. The vibrational coherent superposition created by impulsive excitation would be different for each initial ground-state vibrational level, that is, the thermal distribution yields an inhomogeneity in the ensemble. The vibrational contribution to the polarization response then evolves according to interferences between vibrational superpositions within each molecule but can vary from molecule to molecule throughout the ensemble. The anharmonicity of these modes would provide a faster decay for the vibrational coherences observed here. The present measurements will be influenced by both ground and excited state anharmonicity of each vibrational mode. The significance of wavepacket 'unphasing' due to anharmonicity is not uniquely determined by the pump–probe measurements, but an argument against the significance of this type of broadening can be made by comparison with other experiments.

In the case of molecular iodine, the sequence structure due to anharmonicity for the 110 cm^{-1} B-state vibrational mode causes a decay in the amplitude of the oscillatory feature within 5 ps.[66] However, the oscillations recur and persist for tens of picoseconds. More rapid dephasing of the iodine vibrational coherence occurs in solution, owing to excited state reaction and ground state solvent-induced dephasing, and recurrences are not observed.[8b] This would suggest that the inhomogeneity contribution to the vibrational decay in solution is small. HITCI has two low-wavenumber modes at 120 and 160 cm^{-1} which both decay with time constants of a few hundred fs. A quantitative comparison cannot be made between molecular iodine and HITCI, however, without knowing the relative anharmonicities of the modes. Nevertheless, if the lower wavenumber vibrational coherences in the cyanine dyes were to 'unphase' due to sequence congestion, the anharmonicity would have to be more than an order of magnitude larger than that of iodine. Such a large anharmonicity, however, would enhance coupling to both the solvent and other intramolecular modes as well.

Johnson and Myers[67] have shown through comparison of time domain (RISRS) and resonance Raman

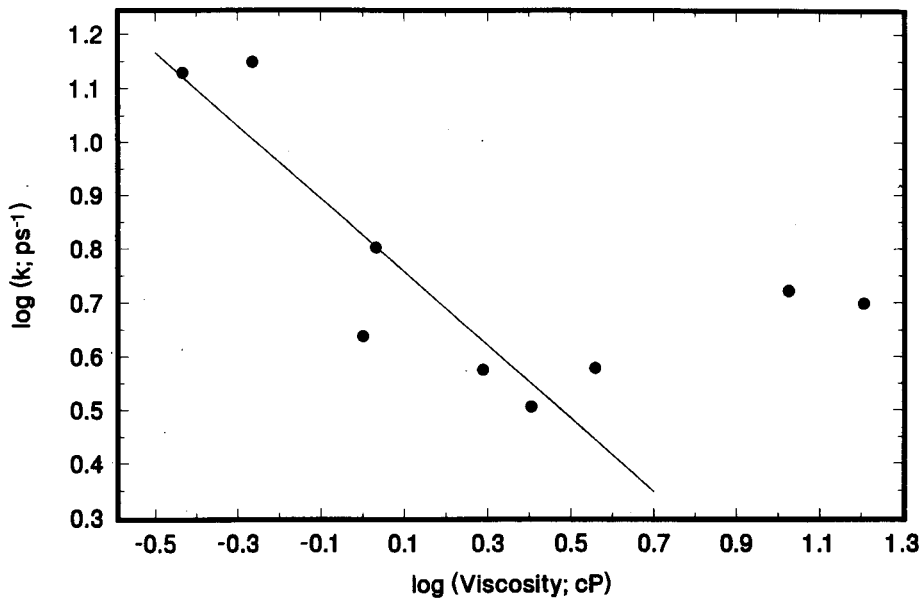

Figure 12. Rate constant vs viscosity. The rate constant is the faster component of the two obtained from a double exponential plus offset fit. The line is a linear least-squares fit through all points accept decanol and ethylene glycol. Line has equation $y = 0.83 \pm 0.05 - (0.68 \pm 0.14)x$.

experiments and wavepacket simulations that sequence congestion is observable in the triiodide ion. This was less apparent in the time domain signal than in the frequency domain. Their comparative study suggests that resonance Raman measurements of the cyanine dyes down to low frequency would be most informative. A three-pulse impulsive 'vibrational echo' measurement may also be useful in sorting out the homogeneous and inhomogeneous vibrational broadening.

CONCLUSION

The present study is unique in having simultaneously examined the relaxation dynamics of many impulsively prepared underdamped vibrational modes within the same solute molecule. The lack of a clear solvent dependence for dephasing of underdamped modes as well as the wavenumber dependences are most directly explained by an intra-chromophore vibrational coupling and relaxation process and intra-chromophore dephasing. This would involve coupling to the large intra-chromophore bath of overdamped low-wavenumber modes. The coupling would depend on the anharmonicity of the underdamped vibrational mode.

The solvent dependence of the exponential decay of the pump–probe signal could result from population relaxation of overdamped oscillator(s) of the chromophore. The inverse relationship between relaxation rate and viscosity is reminiscent of a similar dependence for isomerization reactions. These results indicate that the pertinent molecular vibrational motions behave diffusively. This is an important observation, which is in contrast to the solvent-independent dephasing of underdamped vibrational modes. An important direction for further examination involves elucidation of the microscopic dynamics of this rapid relaxation by comparing the overall relaxation function with the simulated pump–probe signal using measured solvent spectral densities.[20,68] Pressure-dependent studies that examine the variation of the dephasing dynamics with changes in denity would be helpful in better establishing the solvent intermolecular dynamics and effective potentials.

A deeper understanding of liquid dynamics and coupling to the observable coordinate can be obtained from comparison of non-linear response functions and lineshape functions from pump–probe measurements with two- and three-pulse photon echo measurements. Two-pulse echo measurements are not especially sensitive to the Stokes shift parameter but are sensitive to the stochastic description of the magnitude and timescale of solvent fluctuations. The results of electronic coherence will, in conjunction with the present pump–probe measurements, be used to quantify liquid dynamics and interactions. This information can be used to compare with and predict chemical reaction dynamics, such as isomerization and perhaps charge-transfer dynamics, in the same solvents. The objective is to obtain information and a broader perspective from these studies to provide new microscopic details of liquid-phase dynamics and to establish a new basis for the development of more rigorous molecular-level understanding of chemical reactions in liquids.

Acknowledgements

We thank Professor Michael Therien for the use of absorption and emission spectrometers and Professor John Simon for communicating results of pump–probe measurements on HITCI prior to publication. We thank the Deutsche Forschungsgemeinschaft and the US Department of Educational for fellowship support and the National Science Foundation for a National Young Investigator Award. This research was partially supported by a grant from the Petroleum Research Fund of the American Chemical Society. We acknowledge the National Science Foundation for equipment support through grant CHE92-21000 and support from the University of Pennsylvania Materials Research Laboratory through NSF grant DMR91-20668. Finally, we acknowledge an award from the University of Pennsylvania Office of Academic Computing for the purchase the Silicon Graphics workstation used in the simulations. N. F. Scherer is the recipient of a David and Lucile Packard Fellowship.

REFERENCES

1. G. R. Fleming and P. Hängii (Eds), *Activated Barrier Crossing*. World Scientific, River Edge, NJ (1993); G. R. Fleming and P. G. Wolynes, *Phys. Today* **43**, 36 (1990); J. N. Onuchic and P. G. Wolynes, *J. Phys. Chem.* **92**, 6495 (1988).
2. (a) M. Bixon and J. Jortner, *Faraday Discuss. Chem. Soc.* **74**, 17 (1982); (b) M. D. Newton and N. Sutin, *Annu. Rev. Phys. Chem.* **35**, 437 (1984); (c) J. T. Hynes, E. Carter, G. Cicotti, H. J. Kim, D. A. Zichi, M. Ferrario and R. Kapral, in *Perspectives in Photosynthesis*, edited by J. Jortner and B. Pullman, p. 133. Kluwer, Dordrecht (1990).
3. S. Mukamel, *Annu. Rev. Phys. Chem.* **41**, 647 (1990); S. Mukamel, *Adv. Chem. Phys.* **70**, 165 (1988); S. Mukamel and R. F. Loring, *J. Opt. Soc. Am.* **B3**, 595 (1986).
4. J. R. Andrews, R. M. Hochstrasser and H. P. Tromsdorff, *Chem. Phys.* **62**, 87 (1981).
5. T. S. Rose, M. J. Rosker and A. H. Zewail, *J. Chem. Phys.* **88**, 6672 (1988); **91**, 7415 (1989); L. R. Khundkar and A. H. Zewail, *Annu. Rev. Phys. Chem.* **41**, 15 (1990).
6. H. L. Fragnito, J. Y. Bigot, P. C. Becker and C. V. Shank, *Chem. Phys. Lett.* **160**, 101 (1989); R. W. Schoenlein, L. A. Peteanu, R. A. Mathies and C. V. Shank, *Science* **254**, 412 (1991).
7. U. Banin, S. Ruhman, *J. Chem. Phys.* **98**, 4391 (1993); U. Banin, A. Waldman and S. Ruhman, *J. Chem. Phys.* **96**, 2416 (1992).
8. (a) N. F. Scherer, D. Jonas and G. R. Fleming, *J. Chem. Phys.* **99**, 153 (1993); (b) N. F. Scherer, L. D. Ziegler and G. R. Fleming, *J. Chem. Phys.* **96**, 5544 (1992).
9. N. Pugliano, D. K. Palit, A. Z. Szarka and R. M. Hochstrasser, *J. Chem. Phys.* **99**, (1993).
10. M. J. Rosker, F. W. Wise and C. L. Tang, *Phys. Rev. Lett.* **57**, 321 (1986); *J. Chem. Phys.* **86**, 2827 (1987).
11. J. Chesnoy and A. Mokharti, *Phys. Rev. A* **28**, 2566 (1988).
12. (a) Q. Hong, I. A. D. Pexton, G. Porter and D. R. Klug, *J. Phys. Chem.* **97**, 12561 (1993); (b) T. Joo and A. C. Albrecht, *Chem. Phys.* **173**, 17 (1993).
13. K. A. Nelson and E. P. Ippen, *Adv. Chem. Phys.* **75**, 1 (1989).
14. D. McMorrow, W. T. Lotshaw and G. A. Kenny-Wallace, *IEEE J. Quantum Electron* **24**, 443 (1988).
15. D. A. V. Kliner, J. C. Alfano and P. F. Barbara, *J. Chem. Phys.* **98**, 5375 (1993).
16. (a) I. A. Walmsley, M. Mitsunaga and C. L. Tang, *Phys. Rev. A* **38**, 4681 (1988); (b) W. T. Pollard, S.-Y. Lee and R. A.

Mathies, *J. Chem. Phys.* **92**, 4012 (1990); (c) T. J. Kang, J. Yu and M. Berg, *J. Chem. Phys.* **94**, 2413 (1991).
17. Y. S. Bai and M. D. Fayer, *Chem. Phys.* **128**, 135 (1988); a discussion of photon echos in multi-level systems is given by D. J. Tannor and S. A. Rice, in *Understanding Molecular Properties*, edited by J. Avery *et al.*, Reidel, Dordrecht (1987).
18. J.-Y. Bigot, M. T. Portella, R. W. Schoenlein, C. J. Bardeen, A. Migus and C. V. Shank, *Phys. Rev. Lett.* **66**, 1138 (1991); E. J. Nibbering, D. A. Wiersma and K. Duppen, *Phys. Rev. Lett.* **66**, 2464 (1991).
19. (a) D. W. Oxtoby, *Adv. Chem. Phys.*, **40**, 1 (1979); (b) K. S. Schweitzer and D. Chandler, *J. Chem. Phys.* **76**, 2296 (1982); (c) R. K. Wertheimer, *Mol. Phys.* **38**, 797 (1979); (d) M. R. Zakin and D. R. Hershbach, *J. Chem. Phys.* **89**, 2380 (1988).
20. P. Vöhringer, D. Arnett, R. Westervelt, M. Feldstein and N. F. Scherer, *J. Chem. Phys.* **102**, 4027 (1995); D. Arnett, P. Vöhringer, R. Westervelt, M. Feldstein and N. F. Scherer, in *Springer Series in Chemical Physics*, Vol. 60, edited by P. Barbara, p. 482. Springer, Berlin (1994).
21. P. Cong, Y. J. Yan, H. P. Deuel and J. D. Simon, *J. Chem. Phys.* **100**, (1994).
22. F. Krausz, Ch. Spielmann, T. Brabec, E. Wintner and A. J. Schmidt, *Opt. Lett.* **17**, 204 (1992).
23. M. T. Asaki, C. P. Huang, D. Garvey, J. Zhou, H. C. Kapteyn and M. M. Murnane, *Opt. Lett.* **18**, 977 (1993).
24. F. W. Wise, M. J. Rosker, G. L. Millhauser and C. L. Tang, *IEEE J. Quantum Electron* **QE-23**, 1116 (1987); W. Barkhuijsen, R. DeBeer, W. M. M. J. Bovee and D. van Ormondt, *J. Magn. Reson.* **61**, 465 (1985).
25. A. M. Bonch-Bruevich, T. K. Razumova and G. M. Rubanova, *Opt. Spektros.* **35**, 484 (1973); E. N. Kaliteevskaya and T. K. Razumova, *Opt. Spektros.* **43**, 398 (1977).
26. (a) J. P. Fouassier, D. J. Lougnot and J. Faure, *Chem. Phys. Lett.* **35**, 189 (1975); (b) E. G. Arthurs, D. J. Bradley and A. G. Roddie, *Opt. Commun.* **8**, 118 (1973); *Chem. Phys. Lett.* **22**, 230 (1973).
27. S. Speiser and N. Shakkour, *Appl. Phys. B* **38**, 191 (1985).
28. X. R. Zhu and J. M. Harris, *Chem. Phys.* **142**, 301 (1990).
29. S. L. Palfrey and T. F. Heinz, *J. Opt. Soc. Am.* **B2**, 674 (1985).
30. J.-L. Oudar, *IEEE J. Quantum Electron* **19**, 713 (1983).
31. H. Sato, M. Kawasaki, K. Kasatani and M. Katsumata, *J. Raman Spectrosc.* **19**, 129 (1988).
32. D. W. Oxtoby and S. A. Rice, *Chem. Phys. Lett.* **42**, 1 (1976).
33. D. W. Oxtoby, *Adv. Chem. Phys.* **47**, 487 (1981).
34. A. Fendt, S. F. Fischer and W. Kaiser, *Chem. Phys.* **57**, 55 (1981).
35. T.-S. Yang, R. Westervelt, P. Vöhringer and N. F. Scherer, in preparation.
36. N. Mataga, *Bull. Chem. Soc. Jpn.* **36**, 654 (1963).
37. M. Maroncelli and G. R. Fleming, *J. Chem. Phys.* **86**, 6221 (1987).
38. I. D. L. Albert, P. K. Das and S. Ramasesha, *J. Opt. Soc. Am.* **B10**, 1365 (1993).
39. W. P. de Boeij, M. S. Pshenichnikov, K. Duppen and D. A. Wiersma, *Chem. Phys. Lett.* **224**, 243 (1994).
40. P. Vöhringer, D. C. Arnett, T.-S. Yang and N. F. Scherer, *Chem. Phys. Lett.* **237**, 387 (1995).
41. T.-S. Yang, D. C. Arnett, P. Vöhringer and N. F. Scherer, *J. Chem. Phys.*, in press.
42. R. M. Whitnell, K. R. Wilson and J. T. Hynes, *J. Chem. Phys.* **96**, 5354 (1992).
43. P. Hänggi, P. Talkner and M. Borkovec, *Rev. Mod. Phys.* **62**, 251 (1990); H. A. Kramers, *Physica* **7**, 284 (1940).
44. G. Rothenberger, D. K. Negus and R. M. Hochstrasser, *J. Chem. Phys.* **79**, 5360 (1983).
45. R. F. Grote and J. T. Hynes, *J. Chem. Phys.* **73**, 2715 (1980).
46. J. Schroeder, J. Troe and P. Vöhringer, *Chem. Phys. Lett.* **203**, 255 (1993); Ch. Gehrke, R. Mohrschaladt, J. Schroeder, J. Troe and P. Vöhringer, *Chem. Phys.* **152**, 45 (1991); J. Schroeder, D. Schwarzer, J. Troe and P. Vöhringer, *Chem. Phys. Lett.* **218**, 43 (1994).
47. L. Nikowa, D. Schwarzer, J. Troe and J. Schroeder, *J. Chem. Phys.* **97**, 4827 (1992).
48. J. T. Hynes, *Annu. Rev. Phys. Chem.* **36**, 573 (1985).
49. D. Chandler, *J. Stat. Phys.* **42**, 49 (1986).
50. D. E. Smith and C. B. Harris, *J. Chem. Phys.* **87**, 2709 (1987); A. L. Q. Harris, M. Berg and C. B. Harris, *J. Chem. Phys.* **84**, 788 (1986).
51. J. C. Owrutsky, D. Raftery, R. Hochstrasser, *Annu. Rev. Phys. Chem.* **45**, 519 (1994).
52. M. R. Battaglia and P. A. Madden, *Mol. Phys.* **36**, 1601 (1978).
53. S. C. Tucker, *J. Chem. Phys.* **101**, 2006, 1994; S. K. Reese, S. C. Tucker and G. K. Schenter, *J. Chem. Phys.* **102**, 104 (1995).
54. J. D. Simon, *Acc. Chem. Res.* **21**, 128 (1988); P. F. Barbara and W. Jarzeba, *Adv. Photochem.* **15**, 1 (1990).
55. Y. T. Mazurenko, *Opt. Spektrosk.* **48**, 388 (1980); **36**, 283 (1974).
56. B. Bagchi, D. W. Oxtoby and G. R. Fleming, *Chem. Phys.* **86**, 25F (1984).
57. M. Maroncelli, *J. Chem. Phys.* **94**, 2085 (1991).
58. E. A. Carter and J. T. Hynes, *J. Chem. Phys.* **94**, 5961 (1991).
59. S. J. Rosenthal, X. Xie, M. Du and G. R. Fleming, *J. Chem. Phys.* **95**, 4715 (1991).
60. M. Maroncelli, V. P. Kumar and A. Papazyan, *J. Phys. Chem.* **97**, 13 (1993).
61. A. M. Weiner and E. P. Ippen, *Chem. Phys. Lett.* **114**, 456 (1985).
62. D. McQuarrie, *Statistical Mechanics* Harper and Row, London (1976).
63. D. W. Oxtoby, *J. Chem. Phys.* **70**, 2605 (1979).
64. M. Lee, G. R. Holton and R. M. Hochstrasser, *Chem. Phys. Lett.* **118**, 359 (1985).
65. G. R. Fleming, S. H. Courtney and M. W. Balk, *J. Stat. Phys.* **42**, 83 (1985).
66. R. M. Bowman, M. Dantus and A. H. Zewail, *Chem. Phys. Lett.* **161**, 297 (1989).
67. A. E. Johnson, and A. B. Myers, *J. Chem. Phys.* submitted for publication.
68. M. Cho, S. J. Rosenthal, N. F. Scherer, L. D. Ziegler and G. R. Fleming, *J. Chem. Phys.* **96**, 5033 (1992).